Seismic wavefield change preceding the eruption of Shinmoe-dake, Kirishima volcano, Japan, inferred from polarization analysis

Takashi Hirose[1], **Hideki Ueda**[2]

[1]Department of Geophysics, Graduate School of Science, Tohoku University
[2]National Research Institute for Earth Science and Disaster Resilience
[1]6-3, Aramaki Aza-Aoba, Aoba-ku, Sendai, Miyagi, 980-8578, Japan
[2]3-1, Tennodai, Tsukuba, Ibaraki, 305-0006, Japan

Key Points:

- The Rayleigh wave source back azimuths were estimated by polarization analysis of single-station seismograms at the Kirishima volcano.
- At the nearest seismometer to the Shinmoe-dake crater, Rayleigh waves from the crater dominated 7 months before the October 2017 eruption.
- A noticeable increase in the amplitudes of retrograde Rayleigh waves originating from the crater direction was detected since August 2016.

Corresponding author: Takashi Hirose, takashi.hirose.b6@tohoku.ac.jp

Abstract

A volcanic tremor is a seismic event linked to volcanic processes, identified by ongoing ground shaking. While there are different theories regarding the mechanism of volcanic tremors, they play a crucial role in understanding internal volcanic activities and forecasting eruptions. Detecting weak volcanic tremor signals before an eruption has remained a difficult task. This study utilized polarization analysis on continuous seismograms at Kirishima volcano, Japan, to extract data on retrograde Rayleigh wave sources. Back azimuth estimates focused on the direction of the Shinmoe-dake crater before and during the volcanic eruptions in 2011, 2017, and 2018. Rayleigh waves originating from the crater direction, particularly in the 1.3–2.5 Hz band, were observed starting around March 2017, approximately 7 months prior to the October 2017 eruption. In the 1.3–2 Hz band, the back azimuths steadily moved closer to the crater's direction between January and March 2017. A noticeable increase in the amplitudes of retrograde Rayleigh waves from the crater direction was observed starting in August 2016. Enhancing the growth in amplitude was achieved by utilizing a filter on the seismograms. As polarization analysis requires only a single three-component seismometer, this approach allows for the timely identification of weak Rayleigh waves from the crater direction, even in volcanoes with limited seismic station coverage. The results obtained in this study contribute to the growing knowledge on volcanic tremors and their potential use in volcano monitoring and eruption forecasting.

Plain Language Summary

Volcanic tremors, seismic events linked to volcanic activity, are crucial for understanding volcanoes and predicting eruptions. This study focused on Kirishima volcano in Japan, analyzing seismic data to trace Rayleigh wave sources, especially pre-eruption in 2011, 2017, and 2018. Rayleigh waves from the crater direction, with frequencies between 1.3 and 2.5 Hz, were notable around March 2017, months before the October eruption. The study showed Rayleigh wave amplitudes increased from August 2016, and their origin shifted closer to the crater over time. By filtering seismic data, researchers isolated waves from the crater, using a single seismometer, which aids in monitoring with limited stations. These insights advance understanding of volcanic tremors and eruption forecasting.

1 Introduction

Volcanic tremor is a seismic phenomenon associated with volcanic activity, characterized by continuous ground shaking. It is a key signal in volcanology, providing insights into the internal processes of volcanoes and aiding in eruption forecasting. Volcanic tremor is linked to the movement and interaction of magmatic fluids with the surrounding bedrock, and its characteristics can vary widely among different volcanoes. The onset of tremor and its amplitude often correlate directly with volcanic activity, and its frequency spectrum typically shows sharp peaks between 0.1 and 7 Hz, which may represent fundamental frequencies and their harmonics or a random distribution. The tremor can precede or follow eruptions, lasting from minutes to months, and the depth of the source can range from a few hundred meters to tens of kilometers (Konstantinou & Schlindwein, 2002; Burlini et al., 2007). Volcanic tremors offer valuable insights into the internal volcanic processes. The frequency and amplitude of volcanic tremor can change with the intensity of volcanic activity, and these changes can be used to infer the size and dynamics of the volcanic source (Gordeev et al., 1990). Long-period (12 sec) volcanic tremors at Usu volcano correlate with the uplift rate of the eruption area and are attributed to the flow-induced vibration of a magma chamber and its outlet (Yamamoto et al., 2001). The location of tremor sources can migrate over time and may be associated with changes in volcanic activity, potentially altering the conduit conditions (Ichimura et al., 2018).

While volcanic tremors have been widely recognized as short-term (ranging from days to minutes) indicators of volcanic eruptions (Swanson et al., 1985; Hotovec et al., 2013), there have been instances where eruptions have taken place without these evident warning signs (Castruccio et al., 2016; Reckziegel et al., 2016). One possible explanation is that they might be overshadowed by other signals due to the weak energy of their signals (Ichihara et al., 2023). Hence, the early detection of volcanic tremor signals prior to an eruption continues to be difficult. Additionally, in situations where volcanic tremor signals are weak, they might only be captured by a limited number of seismometers near the source of the tremor (Ichihara et al., 2023), highlighting the need for an analysis technique suitable for such scenarios.

Polarization analysis, which can be applied with a single three-component seismogram, has contributed to the advancement of our understanding of wave propagation characteristics and sources. Polarization analysis of long-term continuous seismogram records has been used primarily to study the source of microseisms (Tanimoto et al., 2006; Koper & Hawley, 2010; Takagi et al., 2018). Takagi et al. (2018) applied polarization analysis to Hi-net data and investigated the characteristics of the ambient noise wavefield in Japan over 1 year. The back azimuths of both Rayleigh and P wave sources were sensitive to adjacent oceanic activities and exhibit seasonal directional variations. Long-term polarization analysis of seismic data can help to reveal changes in volcanic activity and potentially indicate changes in source properties. Falsaperla, S., J. Wassermann, and F. Scherbaum (2002) applied polarization analysis to broadband seismic data recorded at Stromboli volcano, Italy, during 1996–1999. They observed statistically significant changes in the wavefield parameters over the long term, ranging from several months to a year. During the period between late 1997 and early 1998, the observed changes were understood as potentially resulting from the increased intensity of a subsurface reservoir, likely due to the influx of fluids from a lower section of the magma conduit. Polarization analysis can be a useful tool for studying seismic signals related to volcanic activity.

Kirishima volcano is a cluster of basaltic-andesite volcanoes located in the southern region of Kyushu, Japan. These volcanoes have shown activity within the last 22,000 years (Kagiyama, 1994; Kato & Yamasato, 2013). Shinmoe-dake has emerged as the most active volcano in the Kirishima group in recent years. The current cycle began with a small phreatic explosion on 19 January 2011. The first magmatic eruption occurred from 26 January 2011 to 27 January 2011 (Nakada et al., 2013). The eruption that took place in 2011 involved sub-Plinian events, the movement of lava, and Vulcanian explosions. It lasted from January 27 to February 7, with a prolonged lava stream reaching about 1.2 km from the crater towards the southeast. Following a subsequent period of inactivity lasting six years, Shinmoe-dake experienced another eruption on October 11, 2017. This marked the first explosive eruption in seven years, with sporadic eruptions persisting until October 17, 2017 (Japan Meteorological Agency, 2017). Volcanic ash emissions and volcanic tremors were observed continuously until October 21, 2017 in this timeframe. Another explosive eruption took place on March 6, 2018, with a total of 47 explosive eruptions documented between March 1 and 9, 2018 (Japan Meteorological Agency, 2018). Throughout this period of eruptive activity, both volcanic ash emissions and lava flows were verified. Between March 10 and June 27, 2018, there were occasional Vulcanian eruptions. Throughout this time, Shinmoe-dake encountered multiple explosive eruptions, releasing volcanic ash into the air. The eruption column rose up to 3,000 m at its peak. During the eruption on June 27, the volcanic ash dispersed towards the southeast, impacting regions on the downwind side. These consecutive eruptive events notably enlarged the crater of Shinmoe-dake. Tracking volcanic tremor activity by polarization analysis in the Kirishima volcano that repeats eruptive and quiescent periods at intervals of several years can provide insights into the internal processes of volcanoes.

This study used polarization analysis on continuous seismograms at the Kirishima volcano to estimate the back azimuth of Rayleigh wave sources. The objective of this

study is to discover variations in the seismic ambient noise wavefield that are associated with volcanic activities.

2 Data and Methods

2.1 Data

Figure 1 displays the location of the Kirishima volcano and the spatial arrangement of the seismic stations. We used the V.KIRA seismic station, which is maintained by the Japan Meteorological Agency (JMA) and positioned closest to the Shinmoe-dake crater (approximately 2 km away). A short-period seismometer with three components and a natural period of 1 s was installed on the ground surface. The seismograms were recorded at a sampling rate of 100 Hz. We analyzed continuous seismograms for the period from January 1, 2011, to December 31, 2022 (a span of 12 years). All continuous seismograms can be accessed at the Data Management Center of the National Research Institute for Earth Science and Disaster Resilience (NIED) (`https://hinetwww11.bosai.go.jp/auth/?LANG=en`).

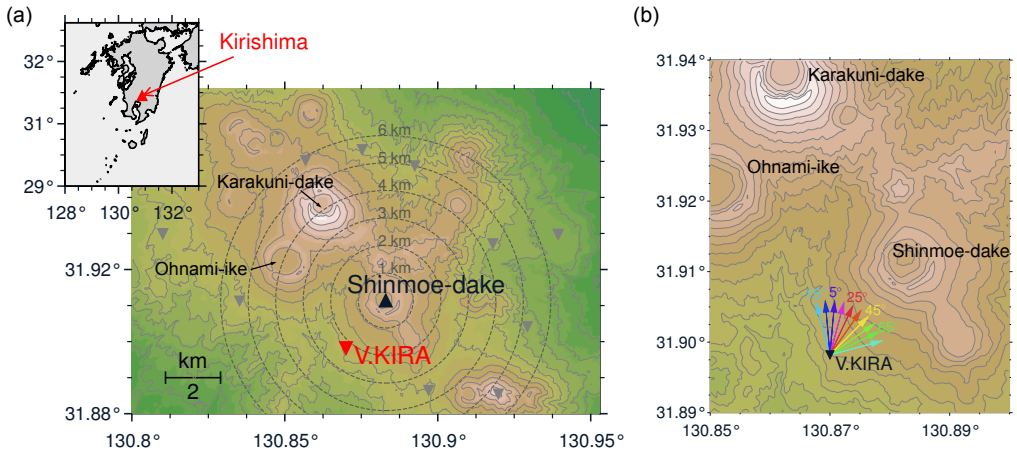

Figure 1. (a) Topographic map of Kirishima volcano and location of the V.KIRA seismic station, which is mainly used in this study (red inverted triangle). The other seismic stations maintained by JMA and NIED are shown by gray inverted triangles. The black triangle represents the Shinmoe-dake crater. Gray contours show elevations with an interval of 100 m. (b) The spatial connection between back azimuth values and the Shinmoe-dake crater's location is illustrated. The hues of each arrow align with the back azimuth colors depicted in Figures 3 and 4.

2.2 Estimation of the dominant back azimuths of Rayleigh wave sources

Polarization properties are valuable instruments for distinguishing and segregating various kinds of waves found in a signal with multiple components. This study focuses on Rayleigh waves and estimates back azimuths of their sources. The polarization state of Rayleigh waves is elliptical, which can be either retrograde or prograde, with a phase difference of $\pm\frac{\pi}{2}$ between the radial and vertical components. In this study, we apply the Stockwell transform (Stockwell et al., 1996) for the mapping between time and time-frequency domains (Meza-Fajardo et al., 2015). The Stockwell transform is an extension of the short-time Fourier transform that utilizes a Gaussian window that can be

moved and scaled. Figure 2 displays the diagrammatic representation of the back azimuth estimation technique. We calculate the dominant back azimuth of the retrograde Rayleigh wave source every 30 minutes: we first calculate the dominant back azimuth for a 2-minute time window and then iterate the estimation by shifting the time window by 1 minute within the 30-minute window.

Details of the data processing are as follows. Initially, we corrected the instrumental response of the seismometers (Maeda et al., 2011) and reduced the sampling rate of the seismograms from 100 to 20 Hz to speed up the calculations. The 30-minute seismogram was then segmented into 2-minute windows with a 50% overlap, and the Stockwell transform was applied to each 2-minute segment $u_\ell(t)$ (ℓ =N, E, V, R, T):

$$S_\ell(\tau, f) = \int_{-\infty}^{\infty} u_\ell(t) \frac{|f|}{\sqrt{2\pi}} \exp\left[-\frac{(\tau - t)^2 f^2}{2}\right] \exp[-2\pi i f t] dt, \tag{1}$$

where τ is the center of the Gaussian window and f represents frequency. The Stockwell transforms of the signal's north, east, and vertical components are represented as $S_N(\tau, f)$, $S_E(\tau, f)$, and $S_V(\tau, f)$, respectively. We recognize that each of the discrete Stockwell transforms is a matrix defined in the discretized (τ, f) space. Moreover, each element $S_\ell(\tau, f)$ of the discretized space is a complex number. The vertical component's two-element vector, for instance, is specified as:

$$\mathbf{V}(\tau, f) = \begin{pmatrix} \mathrm{Re}\left[S_\mathrm{V}(\tau, f)\right] \\ \mathrm{Im}\left[S_\mathrm{V}(\tau, f)\right] \end{pmatrix}. \tag{2}$$

The reference angle of the direction of propagation $\theta_r(\tau, f)$ is calculated as follows:

$$\theta_r(\tau, f) = \tan^{-1}\left[\frac{\mathbf{E}(\tau, f) \cdot \hat{\mathbf{V}}(\tau, f)}{\mathbf{N}(\tau, f) \cdot \hat{\mathbf{V}}(\tau, f)}\right], \quad \left(-\frac{\pi}{2} < \theta_r < +\frac{\pi}{2}\right). \tag{3}$$

Where $\hat{\mathbf{V}}(\tau, f)$ represents the function $\mathbf{V}(\tau, f)$ shifted in phase by $+\frac{\pi}{2}$ in the case of retrograde Rayleigh wave. We assume here that the fundamental-mode Rayleigh wave dominates, and these phases generally show retrograde motions (Tanimoto & Rivera, 2005). The direction of propagation θ is calculated as follows:

$$\theta(\tau, f) = \theta_I + \frac{\pi}{2}\left\{\mathrm{sign}\left[\sin\left(\theta_I\right)\right] - \mathrm{sign}\left(x_{pr}\right)\right\}, \tag{4}$$

in which

$$\begin{aligned} \theta_I(\tau, f) =& \theta_r + \pi\left\{1 - \mathrm{sign}\left[\sin\left(\theta_r\right)\right]\right\} \\ &+ \pi\left\{1 - \mathrm{sign}\left[\cos\left(\theta_r\right)\right]\right\} \mathrm{sign}\left[\sin\left(\theta_r\right)\right]/2. \end{aligned} \tag{5}$$

The value of $\mathrm{sign}\left(x_{pr}\right)$ is 1 (or -1) when the Rayleigh wave is traveling towards the east (or west). It should be noted that we do not have any previous information about the location of the Rayleigh wave source, and the function $\theta(\tau, f)$ is subject to a π ambiguity. We address this uncertainty by computing both instances of $\theta(\tau, f)$ under the assumptions that $\mathrm{sign}\left(x_{pr}\right) = 1$ and $\mathrm{sign}\left(x_{pr}\right) = -1$. Subsequently, we compute the normalized inner product (NIP) between $\mathbf{R}_\theta(\tau, f)$ and $\hat{\mathbf{V}}(\tau, f)$, as well as between $\mathbf{R}_{\theta+\pi}(\tau, f)$ and $\hat{\mathbf{V}}(\tau, f)$, taking into account the propagation in both θ and $\theta + \pi$ directions. The NIP between the radial and vertical components is defined as:

$$\mathrm{NIP}_{\mathbf{R}_\theta \hat{\mathbf{V}}}(\tau, f) = \frac{\mathrm{Re}\left[S_{\mathrm{R}_\theta}(\tau, f)\right] \mathrm{Re}\left[S_{\hat{\mathrm{V}}}(\tau, f)\right] + \mathrm{Im}\left[S_{\mathrm{R}_\theta}(\tau, f)\right] \mathrm{Im}\left[S_{\hat{\mathrm{V}}}(\tau, f)\right]}{\left|\mathbf{R}_\theta(\tau, f)\right| \left|\hat{\mathbf{V}}(\tau, f)\right|}. \tag{6}$$

When retrograde Rayleigh waves are predominant, the NIP value approaches 1. The direction of propagation is ultimately determined by comparing the NIP values, with the one having a higher value being chosen:

$$\theta(\tau, f) = \begin{cases} \theta(\tau, f), & \text{if } \mathrm{NIP}_{\mathbf{R}_\theta \hat{\mathbf{V}}}(\tau, f) \geq \mathrm{NIP}_{\mathbf{R}_{\theta+\pi} \hat{\mathbf{V}}}(\tau, f) \\ \theta(\tau, f) + \pi, & \text{if } \mathrm{NIP}_{\mathbf{R}_\theta \hat{\mathbf{V}}}(\tau, f) < \mathrm{NIP}_{\mathbf{R}_{\theta+\pi} \hat{\mathbf{V}}}(\tau, f) \end{cases}. \tag{7}$$

The back azimuth $\theta_{\text{baz}}(\tau, f)$ is calculated as $\theta_{\text{baz}}(\tau, f) = \theta(\tau, f) + \pi$. The subsequent stage involves determining the dominant back azimuth for the 2-minute window. This is accomplished by computing a circular mean (Mardia & Jupp, 1999) for each frequency.

$$\overline{\theta_{\text{baz}}^{\text{2min}}}(f) = \arg\left(\sum_{j=1}^{n} e^{i\theta_{\text{baz}}(\tau_j, f)}\right). \tag{8}$$

The process is iterated by shifting the 2-minute window by 1 minute. Given that the primary focus of this research is on persistent signals like tremors rather than transient signals like earthquakes, a data processing method is utilized where the back azimuths are averaged every 2 minutes and subsequently averaged over a 30-minute period.

$$\overline{\theta_{\text{baz}}^{\text{30min}}}(f) = \arg\left(\sum_{k=1}^{n} e^{i\overline{\theta_{\text{baz}}^{\text{2min}}}(f)_k}\right). \tag{9}$$

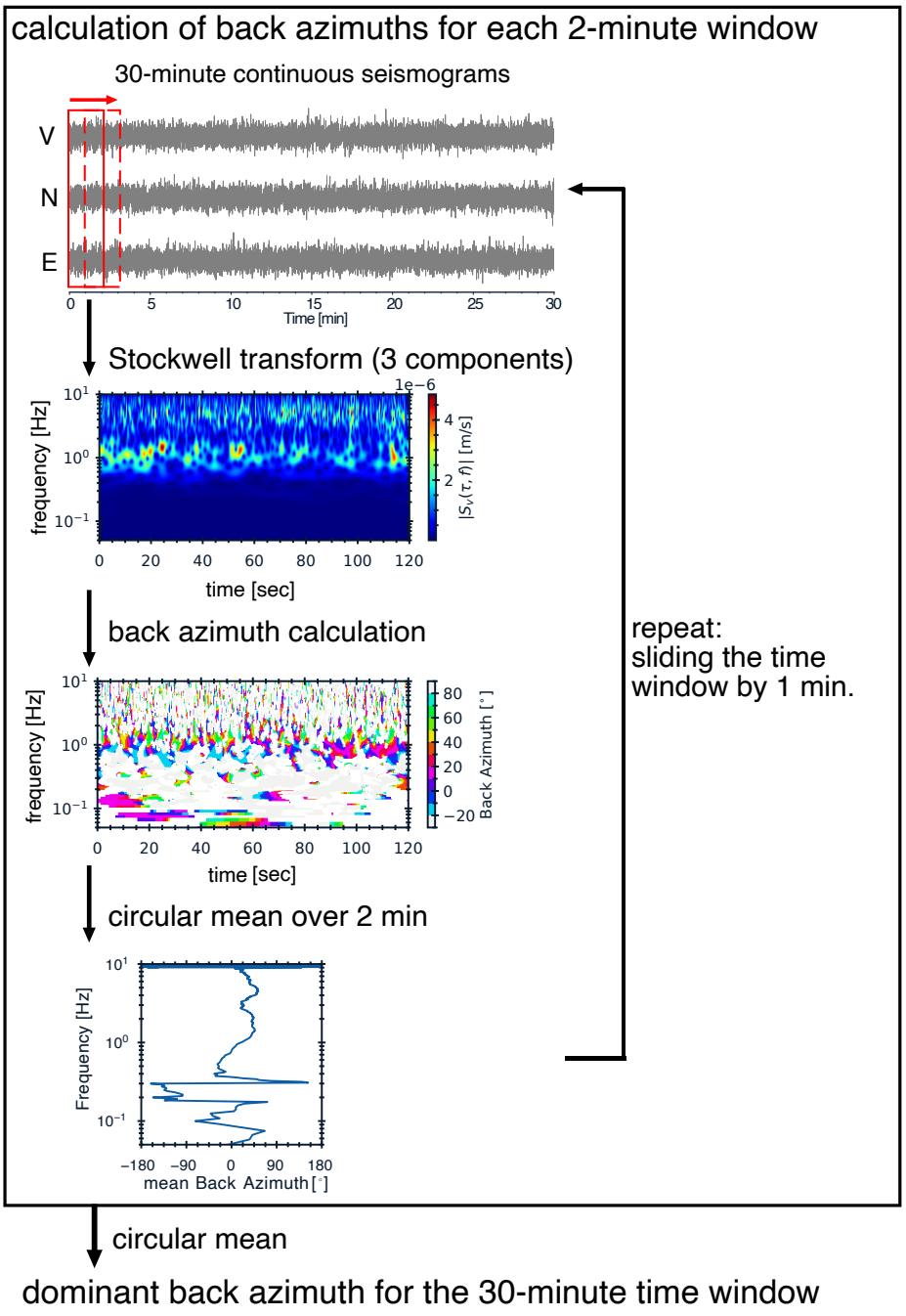

Figure 2. Schematic illustration of estimation method of back azimuth.

3 Results

3.1 Examples of the back azimuth estimation

We present examples of estimating the back azimuth of retrograde Rayleigh waves using seismic data recorded during both eruptive and non-eruptive periods at the Shinmoe-dake crater. Figure 3a illustrates an example of estimating the back azimuth of retrograde Rayleigh waves using 2-minute seismograms from 01:10 on October 15, 2017 (JST) amid the eruptive phase at the V.KIRA seismic station, while Figure 3c shows the same analysis for the data during 01:10–01:12 on January 1, 2017 (JST), when no active volcanic activity was reported. The velocity seismograms on the vertical component for both time periods are illustrated in the first panels of Figures 3a and 3c, respectively. The Stockwell transform spectrograms on the vertical component for both time periods are shown in the second panels of Figures 3a and 3c. The spectrograms clearly demonstrate the difference in the dominant frequencies of seismic waves between the eruptive and non-eruptive periods. During the eruptive phase (Figure 3a), seismic waves exhibit high energy levels within the frequency bands of 0.7–2 Hz and 3–7 Hz, whereas during the non-eruptive period (Figure 3c), the dominant frequencies of recorded seismic waves are notably distinct, with high energy levels in the 0.5–1 Hz band. Higher-frequency seismic waves are more energetic amid the eruptive phase, probably because of volcanic tremor occurrence.

The third panels of Figures 3a and 3c illustrate the calculated back azimuths at each lapse time and frequency for the respective time periods. During the eruptive phase (Figure 3a), the back azimuth is more commonly estimated towards the crater direction, back azimuth of 30°–50° (N30°E–N50°E), at around 1 Hz, likely due to the predominance of volcanic tremors. In contrast, during the non-eruptive period (Figure 3c), back azimuths are typically not estimated in the direction of the crater, except for the 0.05–0.1 Hz band. In the fourth panels of Figures 3a and c, the $\mathrm{NIP}_{\mathbf{R}_\theta \hat{\mathbf{V}}}$ values are displayed for each lapse time and frequency. During the eruptive phase (Figure 3a), the NIP values often surpass 0.9 at approximately 1 Hz, which coincides with the frequency where the dominant back azimuth is calculated towards the crater. In contrast, during the non-eruptive phase (Figure 3c), the NIP values are typically reduced, except for frequencies below 0.1 Hz, indicating the absence of high-energy retrograde Rayleigh waves arriving from the crater at around 1 Hz.

Figures 3b and 3d illustrate the circular mean of back azimuths for every frequency within the 2-minute window for the eruptive and non-eruptive periods, respectively. During the eruptive phase (Figure 3b), the circular means of back azimuth values show a significant focus on the back azimuths ranging from 30° to 50° (crater direction) at frequencies between 1.3 and 2.5 Hz, with a maximum variation of approximately ±8°. In contrast, during the non-eruptive period (Figure 3d), the mean back azimuths in the same frequency band exhibit significant dispersion and do not show a clear focus towards the crater direction.

These results demonstrate the potential of our analysis method for detecting changes in the seismic wavefield related to volcanic activity. In the next subsection, we apply this method to long-term continuous seismic data to investigate temporal variations in the seismic wavefield over the course of multiple eruptive cycles at the Shinmoe-dake crater.

3.2 Long-term polarization analysis results

Analyzing the polarization of continuous seismograms over an extended period, encompassing both eruptive and non-eruptive phases, may enable us to detect variations in the seismic wavefield linked to volcanic activities. Figure 4 shows temporal changes in estimated back azimuths of retrograde Rayleigh wave sources from 2011 to 2022 (12 years). As illustrated in Figure 2, we calculated the dominant back azimuth value every 30 minutes, and in this section, we present the circular mean of these 30-minute back

azimuth values during the night hours (18:00–05:59 JST) to mitigate the impact of human activities (Nakata et al., 2019). Furthermore, by performing such an averaging process, the influence of short-term transient signals will be minimized, and persistent signals like volcanic tremors will be emphasized more.

Throughout the study period, Shinmoe-dake experienced three notable eruptive events. The initial one was the sub-Plinian eruption that took place on January 26, 2011 (Nakada et al., 2013). The back azimuths of retrograde Rayleigh wave sources were determined in the vicinity of the crater's direction from the beginning of January 2011 to early June 2011 within the frequency range of 1.3–8 Hz (Figure 2a). Below the frequency of 1 Hz during the eruptive phase, the back azimuths estimated are mainly directed towards the crater. This pattern was also observed during the eruptions in 2017 and 2018 (refer to Figure 2b). As the seismic data for the V.KIRA station is accessible starting from January 1, 2011, it is not feasible to determine when exactly before the 2011 eruption the retrograde Rayleigh wave source towards the crater became predominant. Nevertheless, the concentration of back azimuth estimates towards the crater has been evident since early January, indicating the possibility of Rayleigh wave excitation events, probably volcanic tremors, occurring in the shallow region beneath Shinmoe-dake. Shinmoe-dake experienced its initial eruption in six years on October 11, 2017, followed by the first explosive eruption since 2011 on March 6, 2018 (Japan Meteorological Agency, 2017, 2018). During these eruptive phases, the back azimuths of retrograde Rayleigh wave sources were estimated toward the crater (see Figure 4b). The dominant frequency range of retrograde Rayleigh waves originating from the crater direction closely resembles that observed during the sub-Plinian eruption of 2011. What stands out is the increasing presence of retrograde Rayleigh waves originating from the crater direction, particularly in the frequency band of 1.3–2.5 Hz, starting around March 2017, approximately 7 months prior to the eruption in October 2017. No eruptions took place at Shinmoe-dake during this period. Between the eruptions in 2017 and 2018, the dominance of retrograde Rayleigh waves from the crater direction persisted. During this interval, Rayleigh waves of higher frequencies (>3 Hz) were more prevalent compared to the period before the 2017 eruption and the 2011 eruption. However, with the onset of the 2018 eruption, these high-frequency Rayleigh waves became less prominent. By the end of May 2018, the estimated source of Rayleigh waves from the crater direction had decreased.

The dominance of retrograde Rayleigh waves originating from the crater direction during the period without eruptions was also observed from August 2013 to April 2014 (Figure 4a) and in 2020–2022 (Figure 4c). A notable increase in seismic amplitudes was observed in 2020 and 2022 at seismic stations located around 1 km from the Shinmoe-dake crater (Japan Meteorological Agency, 2022). The timings of these amplitude increases are in alignment with those of dominance of the retrograde Rayleigh waves that arrive from the direction of the crater. These observations suggest that the dominance of retrograde Rayleigh waves originating from the crater direction during the period without eruptions is related to volcanic activities. A slight inflation of the deep source was observed in 2013 and 2014(Japan Meteorological Agency, 2014). The dominant frequency range of retrograde Rayleigh waves originating from the crater direction is nearly identical to that observed during eruptive phases in the 2020–2021 period. On the contrary, retrograde Rayleigh waves in the 5–8 Hz range are more prevalent from August 2013 to April 2014. The observed variations in the dominant frequency of retrograde Rayleigh waves may be related to various factors. These factors could include the depth of the source, the physical properties of the magma (e.g., viscosity, gas content, and temperature), the geometry and size of the conduit, and the differences in the source processes such as magma ascent, degassing, and fragmentation. The complex interplay of these factors can result in observed variations in the dominant frequency of retrograde Rayleigh waves. A detailed examination of these factors is beyond the scope of this paper and is not discussed further. However, the results presented in this study may provide valuable information

on the excitation processes of volcanic tremors and the dynamic changes of the magma/hydrothermal system in the shallow part of the volcano.

3.3 Polarization analysis results for each frequency band

In order to observe how the estimated back azimuths vary with frequency, we present the back azimuth estimation outcomes for specific frequency ranges. Figure 5 illustrates a histogram of the back azimuth data for 30-minute windows overnight (18:00–05:59 JST) in frequency bands of 1–1.3 Hz, 1.3–2 Hz, 2–2.5 Hz, and 2.5–3 Hz over 12 years. During the period from the sub-Plinian eruption on January 26 to early February, the estimated back azimuths were predominantly focused towards the crater direction at frequencies above 1.3 Hz, suggesting that the volcanic tremor source was located beneath the Shinmoe-dake crater. This level of focus was maintained until the beginning of June.

The results across all frequency bands above 1.3 Hz consistently show a notable clustering of back azimuth estimates for retrograde Rayleigh waves towards the crater direction from shortly before the October 2017 eruption until May 2018. This finding further supports the idea of a volcanic tremor source located beneath the Shinmoe-dake crater during this period. Interestingly, a clustering of back azimuth has been observed towards the crater direction starting from approximately March 2017 within the frequency range of 1.3–2.5 Hz, with the exception of July and August 2017 at 2-2.5 Hz. In the 1.3–2 Hz band, the back azimuths have been steadily moving closer to the crater's direction between January and March 2017: estimated back azimuths were approximately -40° (N40°W) between October and December 2016, and they gradually shifted to 30° (N30°E)with speed of roughly 18°/month. This gradual migration of the possible volcanic tremor source towards the crater in the months leading up to the 2017 eruption is a significant observation. It is worth noting that similar back azimuths were estimated for the period from October to December 2016, as in previous years (e.g., 2013–2015), indicating that the seasonal variation of the sources is predominant during these periods. The factors contributing to this seasonal variation are not well understood and require further investigation. However, it is important to recognize that there was no observed gradual migration of retrograde Rayleigh wave sources towards the crater during the period of 2013–2015, suggesting that the migration observed in 2016–2017 is likely related to changes in volcanic activity rather than seasonal effects.

The results suggest a possible shift in the back azimuth of retrograde Rayleigh wave sources, moving from a northwesterly direction towards the western side of the Shinmoe-dake. This shift in the location of the volcanic tremor source, as inferred from the back azimuth estimates across multiple frequency bands, provides valuable insights into the changes in volcanic activity leading up to the 2017 eruption. Although the seasonal variation of sources cannot be entirely ruled out, the gradual migration of the tremor source towards the crater, particularly in the 1.3–2 Hz band, suggests a link to the evolving volcanic processes beneath the Shinmoe-dake crater.

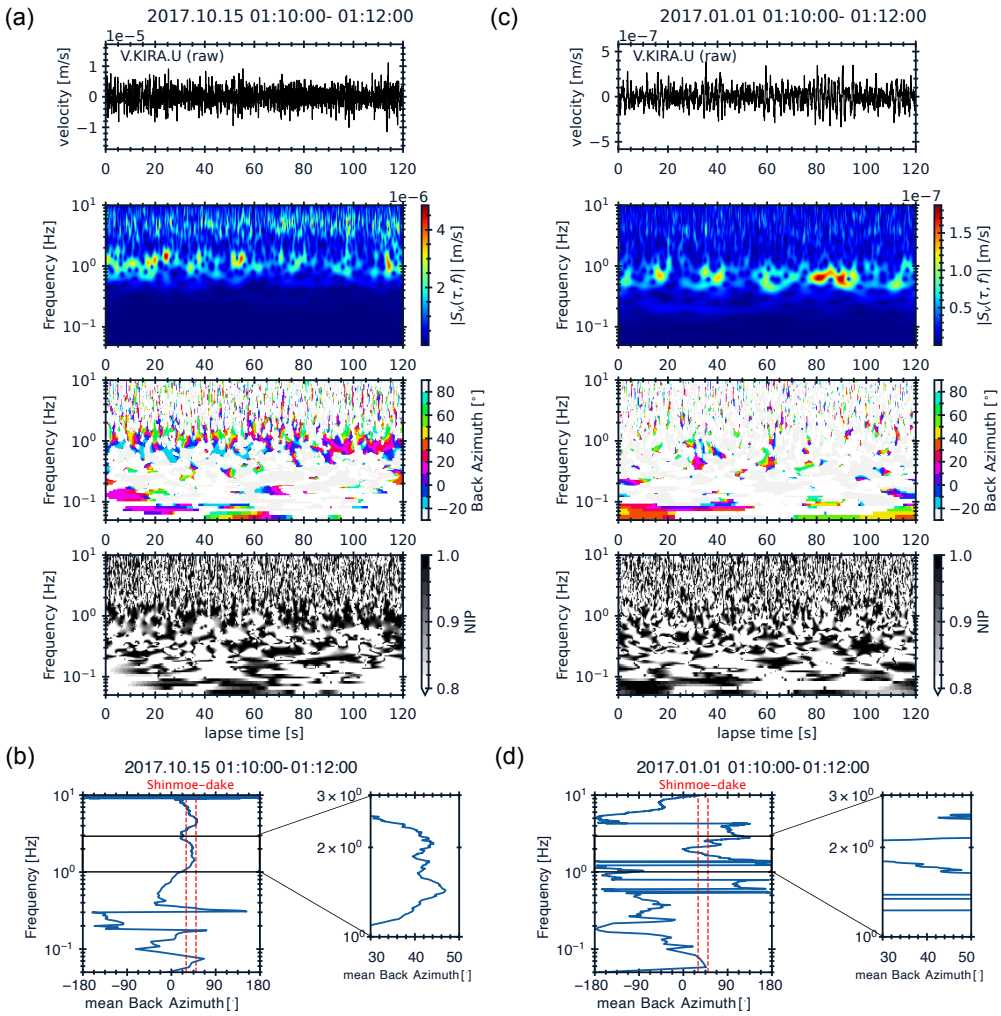

Figure 3. Examples of the back azimuth estimation of retrograde Rayleigh waves for 2-minute-long seismograms. (a) The result of 01:10-01:12 on October 15, 2017. (a1) Velocity seismogram on the vertical component at the V.KIRA seismic station. (a2) Stockwell transform spectrograms on the vertical component. (a3) Estimated back azimuths for each lapse time and frequency. The regions are depicted in white to indicate a normalized inner product (NIP) value lower than 0.8. (a4) NIP values for each lapse time and frequency. (b) Mean back azimuths for each frequency for the time period from 01:10 to 01:12 on October 15, 2017. These values were determined by taking the average of the estimated back azimuths shown in the third panel of (a) across the lapse time. The smaller panel on the right of (b) provides a detailed view. The red vertical dashed lines indicate the back azimuth range of the Shinmoe-dake crater (N30°E–N50°E). (c)–(d) Similar to (a) and (b), respectively, but for 01:10-01:12 on January 1, 2017.

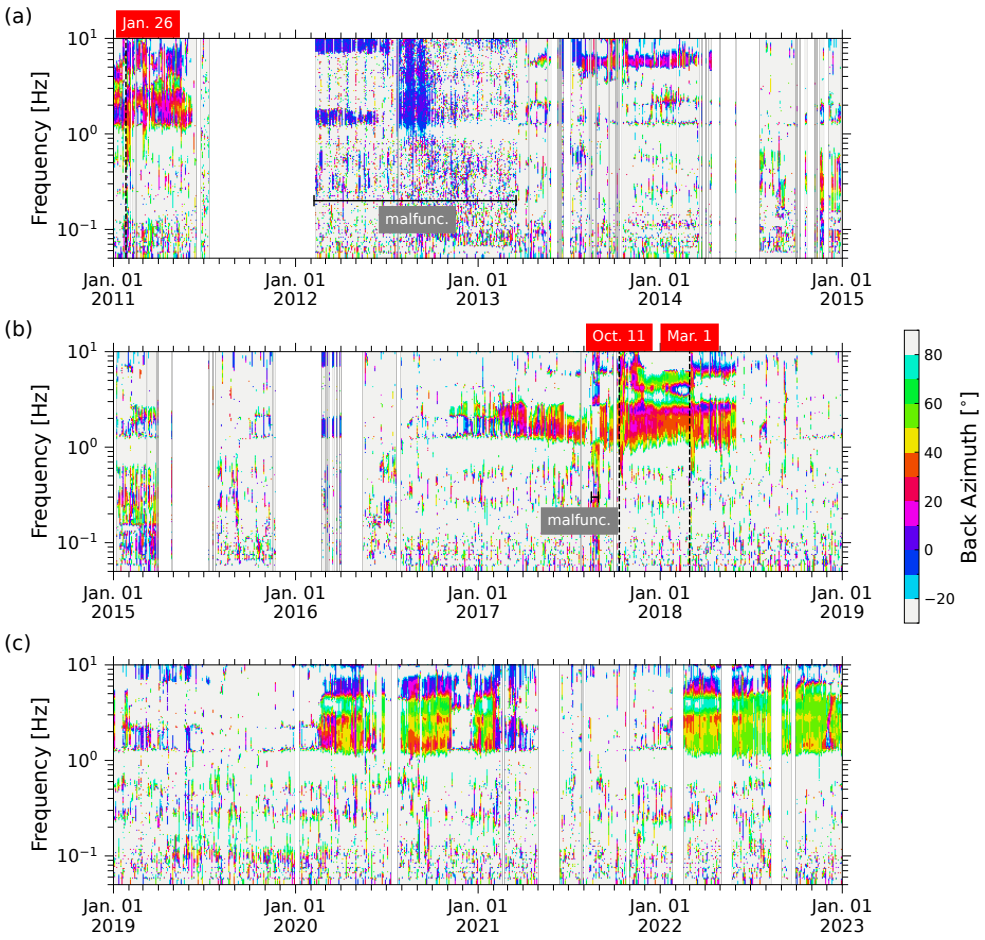

Figure 4. Temporal changes in the estimated back azimuths between 0.05–10 Hz at the V.KIRA seismic station over 12 years. The vertical dashed line in black indicates the occurrence of the sub-Plinian eruption of Shinmoedake on January 26, 2011, as well as the eruptions on October 11, 2017, and March 1, 2018. The seismometer is believed to have experienced malfunctions from around February 2012 to March 2013 and in late August 2017.

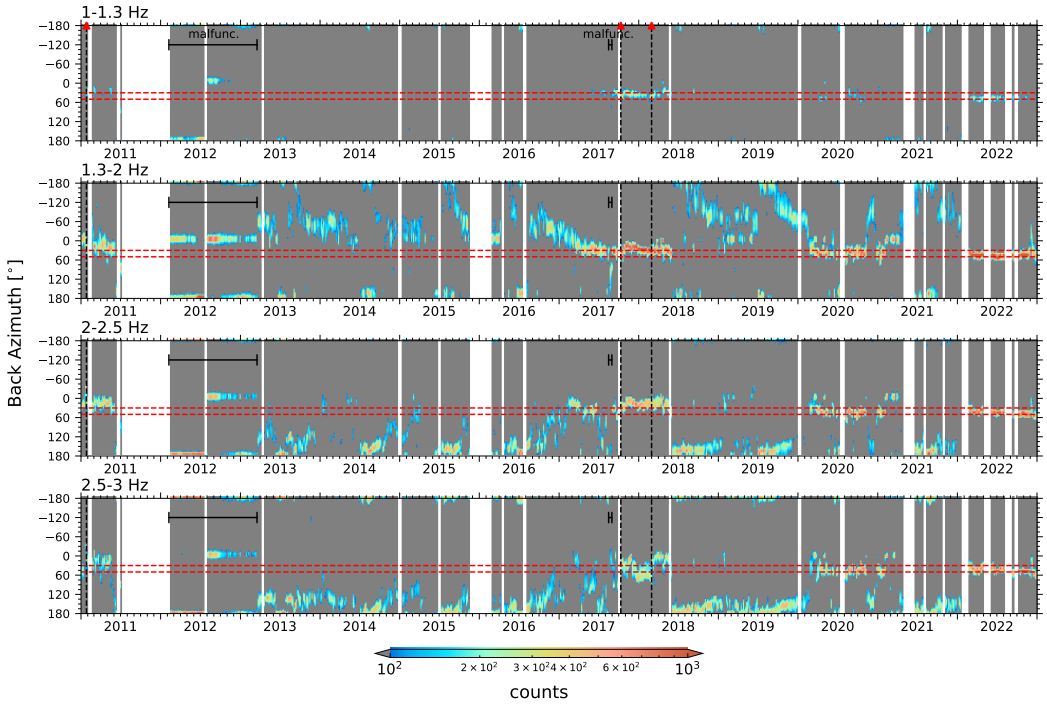

Figure 5. Temporal changes in the daily distribution of back azimuths during nighttime over 12 years. The vertical lines marked with black dashes and red stars indicate the occurrence of eruptions on January 26, 2011, October 11, 2017, and March 1, 2018. The red dashed lines running horizontally indicate the back azimuth aligned with the Shinmoe-dake crater's direction, back azimuths of 30°–50° (N30°E–N50°E). Regions shaded in gray denote counts below 100, while gaps in the data are depicted in white.

4 Discussions

In the Discussion section, we first compare the results of this study with those of previous studies at the Kirishima volcano (4.1). Then, we suggest a candidate for the Rayleigh wave sources mechanism (4.2). Finally, we discuss the implications of our polarization analysis for volcano monitoring (4.3).

4.1 Comparison with results of previous studies

4.1.1 Seismic wave amplitudes growth

In the Results section, our attention is directed towards the temporal variations in the back azimuths of retrograde Rayleigh wave sources, revealing alterations occurring before Shinmoe-dake eruptions. On the other hand, a previous study reported precursory changes in seismic amplitude before the 2017 Shinmoe-dake eruption (Ichihara et al., 2023). They introduced the "seismic background level (SBL)", the root-mean-squared (RMS) amplitude of the seismogram during night. The SBL indicates the amplitude level in quiet time for each day. They observed a rise in SBL preceding the eruptions of Shinmoe-dake in 2011, as well as those in 2017 and 2018, at seismic stations located approximately 1 km away from the Shinmoe-dake crater. Here, we discuss temporal changes in the amplitude of retrograde Rayleigh waves that arrive from the direction of the Shinmoe-dake crater.

Meza-Fajardo et al. (2015) introduced the "Normalized Inner Product (NIP) filter" to extract Rayleigh waves originating from the epicenter of an earthquake. Applying this filter to continuous seismograms can allow us to extract Rayleigh waves originating from the crater. We use this filter in the calculation of the RMS amplitudes of retrograde Rayleigh waves that arrive from the direction of the Shinmoe-dake crater. The NIP filter is defined as follows (Meza-Fajardo et al., 2015):

$$F_\theta(x) = \begin{cases} 0, & x < x_r - \Delta x \\ \frac{1}{2}\cos\left[\frac{\pi(x-x_r)}{\Delta x}\right] + \frac{1}{2}, & x_r - \Delta x < x < x_r \\ 1, & x_r < x \end{cases}. \tag{10}$$

Where $x = \mathrm{NIP}_{\mathbf{R}_\theta,\hat{\mathbf{V}}}$, θ represents the radial direction (i.e., direction of propagation of Rayleigh wave), x_r is the threshold of the NIP value, and Δx is the width of the cosine taper. We used θ =-140° (representing the propagation direction from the Shinmoe-dake crater to V.KIRA), which corresponds to the reverse direction of the back azimuth. We defined x_r =0.8 and Δx =0.1 to construct the filter.

We calculated SBLs using NIP filtered continuous seismograms. The SBL for the V.KIRA seismic station is determined by computing the RMS amplitudes of the seismograms on the vertical component within a 2-minute window in 1.3–2 Hz and 2–2.5 Hz bands. These frequency bands correspond to the range where retrograde Rayleigh sources were identified towards the crater both prior to and following the eruptions (Figure 5). Daily SBL was determined by averaging the bottom 20% values of the 2-minute RMS amplitudes. The blue lines in Figure 6a show the temporal changes in the SBL for the retrograde Rayleigh waves originating from the crater between 2016 and 2018. A 9-day median filter was used on daily SBLs to reduce daily fluctuations, which were then normalized based on the SBL measurement on August 1, 2018. The decrease in SBL levels towards the end of August 2017 could be attributed to a malfunction in the seismometer. For comparison, we also calculated the ordinary SBLs (i.e., SBLs without NIP filtering) in the same manner (gray lines in Figure 6a). The increase in SBL with NIP filtering before the 2017 eruption is more substantial when compared to SBL without NIP filtering. In the frequency band of 1.3–2 Hz, the SBL value using NIP filtering had already increased to 1.8 times its value on August 1, 2016, by June 1, 2017, whereas the SBL value without NIP filtering was around 1.2 times higher. Furthermore, the SBL values obtained with NIP filtering demonstrate a steady increase in comparison to those without NIP filtering within the frequency band of 2 to 2.5 Hz. Specifically, the SBL values without NIP filtering in the 2–2.5 Hz band do not exhibit a noticeable increase until mid-June 2017, whereas those with NIP filtering begin to show an increase from August 2016. In contrast to the scenario lacking NIP filtering, a notable characteristic is the considerable size of the SBL with NIP filtering during the time frame between the 2017 and 2018 eruptions in comparison to the period before the eruptions.

As shown in the Results section, the estimated back azimuths in the 1.3–2 Hz band have been steadily moving closer to the crater direction between January and March 2017 (Figure 5). The growth of SBL with the NIP filter shown in the top panel of Figure 6a possibly reflect the migration of retrograde Rayleigh wave sources. Figure 6b shows temporal changes in SBLs for various back azimuths in the 1.3–2 Hz and 2–2.5 Hz bands. The blue line is the same as that in Figure 6a, and the orange line represents SBL for retrograde Rayleigh waves with a source in the N40°W direction. SBLs in the 1.3–2 Hz band, which shows migration of retrograde Rayleigh wave sources , The SBL values for θ_{baz}=-40° are slightly greater than those for θ_{baz}=40° (crater direction) until February 2017. On the contrary, the SBL values for θ_{baz}=40° starting from March 2017 are significantly higher than those for θ_{baz}=-40°. These results suggest that the migration of retrograde Rayleigh wave sources could have influenced the increase in SBL for θ_{baz}=40°.

For the amplitude growth of retrograde Rayleigh waves arriving from the crater direction, it is difficult to evaluate the effect of migration of the retrograde Rayleigh wave

sources separately from the intensity change of the Rayleigh wave excitation itself. However, the results shown in this subsection suggest that the NIP filter is useful for detecting weak Rayleigh waves that arrive from the crater direction.

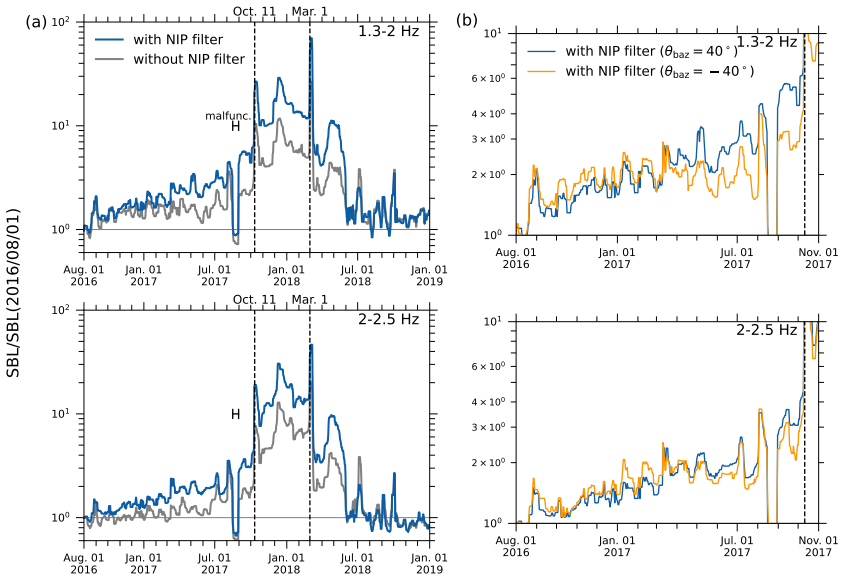

Figure 6. (a) Temporal changes in SBLs at V.KIRA for 1.3–2 Hz and 2–2.5 Hz bands. The 9-day median filter was applied to the daily SBL time series and these time series are then normalized by the value on August 1, 2016. The SBLs were computed and shown as blue lines after the NIP filter was used for θ=-140°, indicating the direction of propagation from the Shinmoedake crater to the V.KIRA. Gray lines represent the SBLs without NIP filtering. The vertical dashed black lines represent the timings of the 2017 and 2018 Shinmoedake eruptions. (b) Temporal changes in SBLs with the NIP filter for various θ values. Note that the ranges of the x-axis and y-axis are different from the panel (a).

4.1.2 Tremor locations

Previous studies estimated the locations of the tremor source that occurred around the Shinmoe-dake. Nakamichi et al. (2013) estimated a location of volcanic tremor sources in early February 2011 by using seismic array data at a site 5 km east of Shinmoe-dake. The continuous tremor source was estimated between Karakuni-dake, Ohnami-ike, and Shinmoe-dake (see Figure 1) at depths between 1 km below sea level and 1 km above sea level. Estimated back azimuths of retrograde Rayleigh wave sources in this study are approximately 20° between 1.3 and 2.5 Hz for the end of February 2011 (Figure 5). Hence, the findings of this study align with the results of Nakamichi et al. (2013) indicating that the continuous tremor source was located on the western side of the Shinmoe-dake. Ichihara et al. (2023) estimated the locations of tremor sources that represent high SBL by utilizing the amplitude-based method for source location within the frequency range of 3.5–7 Hz. Tremor sources related to the 2011 eruption and the 2017-2018 eruptions are located in a comparable area beneath the Shinmoe-dake. By analyzing the SBL ratio for stations located west and north of Shimoe-dake, they found that the tremor sources before the 2011 and 2017 eruptions were shallower and located further to the west compared to the tremors before the 2018 eruption. These results suggest that volcanic tremor sources are distributed in a shallow region beneath/around the Shinomoe-dake. Our find-

412 ings that Rayleigh waves from the crater's direction are significantly dominant before
413 and during the eruption are in line with the results of previous studies that estimated
414 the sources of volcanic tremors in shallow regions around Shinmoe-dake. Because the lo-
415 cations of the tremor sources estimated by these previous studies are shallow, the Rayleigh
416 waves detected in this study probably originate from these tremors.

417 #### *4.1.3 Geodetic deformations*

418 Geodetic deformations caused by the deep pressure source and shallow ones beneath
419 the Kirishima volcano have been revealed by GNSS and interferometric synthetic aper-
420 ture radar (InSAR) analyses. Japan Meteorological Agency (2017) reported an exten-
421 sion of the GNSS baseline at the Kirishima volcano from June 2017. This baseline change
422 originates from the inflation of the deep pressure source located 5 km to the northwest
423 of the summit at a depth of 8 km (Nakao et al., 2013). The back azimuth of the retro-
424 grade Rayleigh wave source, which is speculated to be located in shallow regions, was
425 concentrated in the direction of the Shinmoe-dake crater since about 3 months before
426 the GNSS baseline extension (Figures 4 and 5). Moreover, the increase in SBLs of the
427 retrograde Rayleigh wave from the crater direction also preceded the extension of the
428 baseline (Figure 6). These observations suggest that the volcanic process just beneath
429 the Shinmoe-dake and changes in deeper regions are not completely synchronized.

430 Temporal changes in the shallow pressure source were revealed by using InSAR time-
431 series analysis. Yunjun et al. (2021) reported ∼5 cm inflation of the western flank of the
432 Shinmoe-dake prior to the 2017 eruption. In the LOS time series, inflation appears to
433 have become more pronounced since March 2017, which is consistent with our polariza-
434 tion analysis results and the SBL changes. They explained this inflation by assuming an
435 ellipsoidal pressure source at ∼700 m depth beneath the Shinmoe-dake. Their results
436 are observational facts supporting the hypothesis that volcanic activity changed in the
437 shallow area directly beneath the Shinmoe-dake before the 2017 eruption, and multiple
438 observational terms support the change in volcanic activity in the shallow region of Shinmoe-
439 dake. The results of polarization analysis in this study indicate the possibility of detect-
440 ing changes in volcanic activity in the shallow part of the volcano just beneath the Shinmoe-
441 dake.

442 ### 4.2 Candidate for Rayleigh wave source mechanism

443 Volcanic tremor may be caused by fluid-flow-induced oscillations in conduits, res-
444 onance of fluid-filled cracks, bubble dynamics due to hydrothermal boiling, or oscillations
445 of magma bodies with varying geometries (Konstantinou & Schlindwein, 2002). The depth
446 of the tremor source estimated by Nakamichi et al. (2013) was located in a low resistiv-
447 ity layer, suggesting that hydrothermal processes are a more plausible mechanism for the
448 generation of the tremor. They interpreted that the weak continuous tremor may have
449 been caused by the boiling of water in the heated water-saturated layer (Leet, 1988; Can-
450 nata et al., 2010). Ichihara et al. (2023) references the explanation of how tremors are
451 produced as discussed in the study by Jolly et al. (2020). Jolly et al. (2020) observed a
452 gradual development of faint and ongoing tremors associated with the establishment of
453 the quiet dome on White Island, New Zealand. They explained that the occurrence of
454 these weak and continuous tremors was a result of the interaction between the hydrother-
455 mal system and the slowly propagating magma. Since the results of this study are con-
456 sistent with the results of Nakamichi et al. (2013) and Ichihara et al. (2023), those mech-
457 anisms are also likely candidates for the Rayleigh wave generation mechanism that pre-
458 ceded the eruption captured in this study.

4.3 Seismic wavefields during daytime

To highlight the differences in seismic wavefield characteristics between day and night, we present histograms of estimated back azimuths for day (06:00–17:59 JST) and night (18:00–05:59 JST) separately. Figure 7a (7b) illustrates daily histograms of estimated back azimuths at day and night in the 1.3–2 (2–2.5) Hz band throughout the study period. The results show a clear difference in back azimuth distributions between day and night, except for the period from March 2017 to March 2018, where the distributions are relatively similar. The difference in back azimuth distributions can be attributed to the influence of cultural noise, mainly from human activities, which is predominant above 1 Hz during daytime. This noise typically propagates as surface waves and attenuates within several kilometers (Nakata et al., 2019). Consequently, nighttime data analysis is more effective in detecting retrograde Rayleigh waves from the crater direction.

It is important to note that although our polarization analysis is specifically designed for Rayleigh waves, this approach can be applied even if only one three-component seismometer is deployed. This makes the method useful for monitoring volcanoes, particularly those with a small number of seismic stations. However, caution should be exercised when interpreting daytime data due to the increased influence of cultural noise. In conclusion, the proposed polarization analysis method demonstrates its effectiveness in detecting weak Rayleigh waves from the crater direction, especially during nighttime. Despite its limitations, this single-station approach has the potential to contribute to improved monitoring of volcanoes with limited seismic station coverage. Further research is needed to develop strategies for mitigating the influence of cultural noise and enhancing the applicability of the method to daytime data.

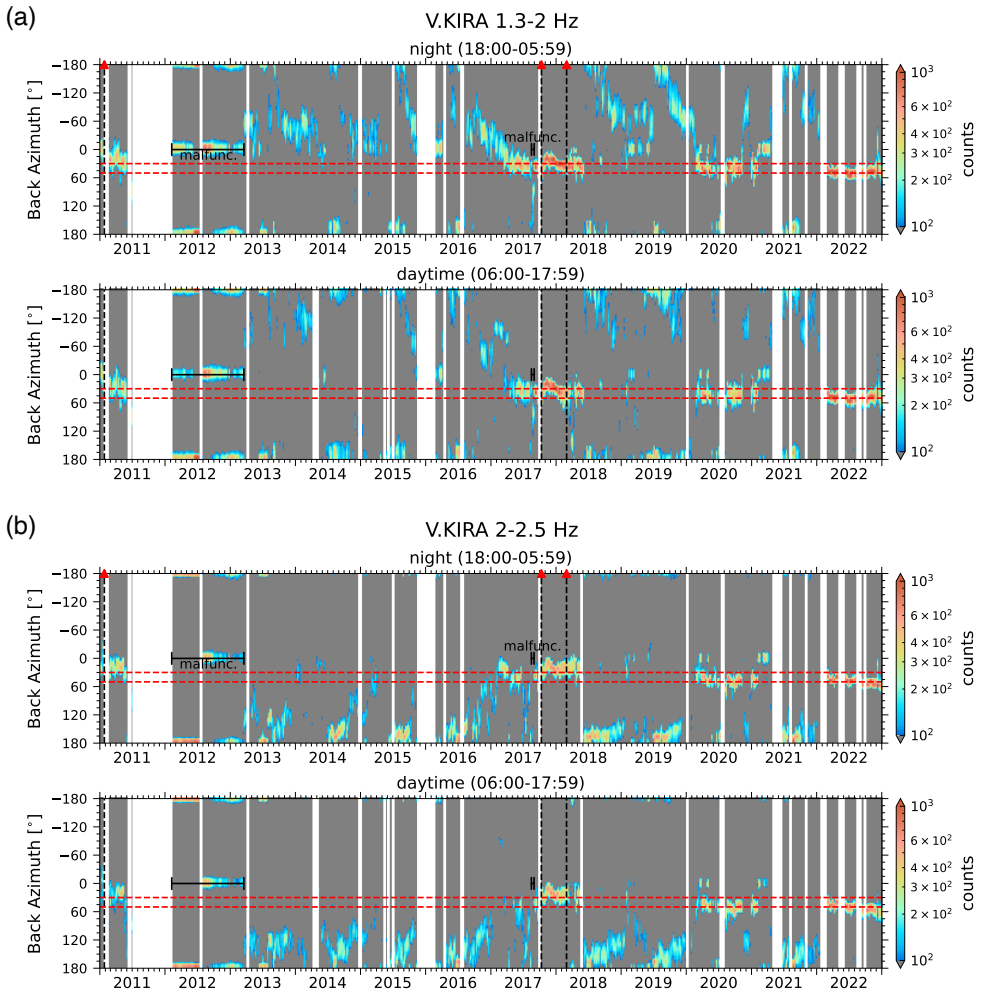

Figure 7. Temporal changes in daily histograms of back azimuths during night and daytime over 12 years at the (a) 1.3–2 Hz and (b) 2–2.5 Hz bands.

5 Conclusion

This study demonstrated the effectiveness of polarization analysis using continuous seismograms for investigating volcanic tremors, which are crucial for advancing our understanding of the internal processes of volcanoes and predicting eruptions. By applying this method to the Kirishima volcano in Japan, we aimed to reveal the temporal changes in the seismic wavefield associated with volcanic activities and to evaluate the potential of this approach for the early detection of precursor signals. The back azimuths of retrograde Rayleigh wave sources were estimated from January 2011 to December 2022 (12 years). Three significant eruptive activities occurred at the Shinmoe-dake crater during our study period, and this allowed us to study temporal changes in back azimuths before and after the eruptions. The estimated back azimuths of retrograde Rayleigh wave sources during nighttime were clearly concentrated in the direction of the Shinmoe-dake crater before and after the 2011, 2017, and 2018 eruptions in the frequency band of 1.3–2.5 Hz. In the case of the 2011 January eruption, this concentration was estimated from early January and continued until early June 2011. In the case of the 2017

October eruption, weak retrograde Rayleigh wave signals that arrived from the crater direction were detected from March 2017, and the concentrations of back azimuths lasted until the end of May 2018, 3 months since the 2018 March eruption. Retrograde Rayleigh wave sources in the 1.3–2 Hz band migrated prior to the 2017 October eruption. The estimated back azimuths were -40° (N40°W) between October and December 2016 and gradually shifted to the western flank of the Shinmoe-dake crater direction (back azimuth=30°, N30°E) with speed of roughly 18°/month. We applied the NIP filter to extract retrograde Rayleigh waves that arrived from the direction of the crater and calculated the seismic background levels (SBLs) (i.e., RMS amplitudes during the night) of these Rayleigh waves. The growth of retrograde Rayleigh waves from the crater direction was estimated since August 2016. In the 1.3–2 Hz band, the SBL value using the NIP filter had already increased to 1.8 times its value on August 1, 2016, by June 1, 2017 (four months before the eruption), while the SBL value without the NIP filter was around 1.2 times higher. This indicates that NIP filtering could be beneficial in detecting weak Rayleigh wave signals from the crater earlier. The results obtained in this study show that the retrograde Rayleigh wave sources approached the crater direction and increased in amplitude as the 2017 eruption approached. These findings may contribute to the assessment of the imminence of volcanic eruptions. Although our polarization analysis is only applicable to Rayleigh wave data, this single-station-based approach will contribute to improving monitoring at volcanoes with a small number of seismic stations. Furthermore, improving the detection capability of weak Rayleigh waves (volcanic tremors) originating in shallow regions of volcanoes is important. This can contribute to a better understanding of the internal processes of volcanoes, regardless of the number of seismometers.

6 Open Research

Continuous seismograms are available from the Data Management Center of the NIED (`https://hinetwww11.bosai.go.jp/auth/?LANG=en`). DEM data, the ALOS Global Digital Surface Model "ALOS World 3D - 30m (AW3D30)," used to create a topographic map, are available at `https://www.eorc.jaxa.jp/ALOS/en/dataset/aw3d30/aw3d30_e.htm`. The "pycpt" package (`https://github.com/j08lue/pycpt`) was used to make color maps in some figures. Data and scripts for creating the figures are available at `https://zenodo.org/doi/10.5281/zenodo.10884533`; Hirose, (2024).

Acknowledgments

We thank the Japan Meteorological Agency (JMA) for providing seismograms. T.H. was supported by JSPS KAKENHI, Grant 20K14581.

References

Burlini, L., Vinciguerra, S., Toro, G. D., Natale, G. D., Meredith, P., & Burg, J. (2007). Seismicity preceding volcanic eruptions: New experimental insights. *Geology*, *35*, 183-186. doi: 10.1130/G23195A.1

Cannata, A., Di Grazia, G., Montalto, P., Ferrari, F., Nunnari, G., Patanè, D., & Privitera, E. (2010). New insights into banded tremor from the 2008–2009 mount etna eruption. *Journal of Geophysical Research: Solid Earth*, *115*(B12).

Castruccio, A., Clavero, J., Segura, A., Samaniego, P., Roche, O., Le Pennec, J.-L., & Droguett, B. (2016). Eruptive parameters and dynamics of the april 2015 sub-plinian eruptions of calbuco volcano (southern chile). *Bulletin of Volcanology*, *78*(9), 62.

Falsaperla, S., J. Wassermann, and F. Scherbaum. (2002). Polarization analyses of broadband seismic data recorded on stromboli volcano (italy) from 1996 to 1999. *Geophys. Res. Lett.*, *29*(10).

Gordeev, E., Saltykov, V., Sinitsyn, V., & Chebrov, V. (1990). Temporal and spatial characteristics of volcanic tremor wave fields. *Journal of Volcanology and Geothermal Research*, *40*, 89-101. doi: 10.1016/0377-0273(90)90108-R

Hotovec, A. J., Prejean, S., Vidale, J., & Gomberg, J. (2013). Strongly gliding harmonic tremor during the 2009 eruption of redoubt volcano. *Journal of Volcanology and Geothermal Research*, *259*, 89-99. doi: 10.1016/J.JVOLGEORES.2012.01.001

Ichihara, M., Ohminato, T., Konstantinou, K. I., Yamakawa, K., Watanabe, A., & Takeo, M. (2023). Seismic background level (SBL) growth can reveal slowly developing long-term eruption precursors. *Sci. Rep.*, *13*(1), 5954.

Ichimura, M., Yokoo, A., Kagiyama, T., Yoshikawa, S., & Inoue, H. (2018). Temporal variation in source location of continuous tremors before ash–gas emissions in january 2014 at aso volcano, japan. *Earth, Planets and Space*, *70*, 1-15. doi: 10.1186/s40623-018-0895-4

Japan Meteorological Agency. (2014). *Volcanic activities of Kirishima during 2014 (in Japanese).* `https://www.data.jma.go.jp/vois/data/tokyo/STOCK/monthly_v-act_doc/fukuoka/2014y/505_14y.pdf`. (Online; accessed 27 February 2024)

Japan Meteorological Agency. (2017). *Volcanic activities of Kirishima during 2017 (in Japanese).* `https://www.data.jma.go.jp/svd/vois/data/tokyo/STOCK/monthly_v-act_doc/fukuoka/2017y/505_17y.pdf`. (Online; accessed 27 February 2024)

Japan Meteorological Agency. (2018). *Volcanic activities of Kirishima during 2018 (in Japanese).* `https://www.data.jma.go.jp/svd/vois/data/tokyo/STOCK/monthly_v-act_doc/fukuoka/2018y/505_18y.pdf`. (Online; accessed 27 February 2024)

Japan Meteorological Agency. (2022). *(1) Kirishima-yama. Documents for the 151th meeting of the coordinating committee for prediction of volcanic eruptions (in Japanese).* `https://www.data.jma.go.jp/svd/vois/data/tokyo/STOCK/kaisetsu/CCPVE/shiryo/151/151_1-9.pdf`. (Online; accessed 27 February 2024)

Jolly, A., Caudron, C., Girona, T., Christenson, B., & Carniel, R. (2020, April). 'silent' dome emplacement into a wet volcano: Observations from an effusive eruption at white island (whakaari), new zealand in late 2012. *Geosci. J.*, *10*(4), 142.

Kagiyama, T. (1994). Kirishima volcanoes-multi active volcanic group generated in a slightly tensile stress field. *Journal of Geography (Chigaku Zasshi)*, *103*(5), 479-487.

Kato, K., & Yamasato, H. (2013). The 2011 eruptive activity of shinmoedake volcano, kirishimayama, kyushu, japan—overview of activity and volcanic alert level of the japan meteorological agency—. *Earth, Planets and Space*, *65*(6), 489–504.

Konstantinou, K., & Schlindwein, V. (2002). Nature, wavefield properties and source mechanism of volcanic tremor: a review. *Journal of Volcanology and Geothermal Research*, *119*, 161-187. doi: 10.1016/S0377-0273(02)00311-6

Koper, K. D., & Hawley, V. L. (2010). Frequency dependent polarization analysis of ambient seismic noise recorded at a broadband seismometer in the central united states. *Earthquake Science*, *23*, 439–447.

Leet, R. C. (1988). Saturated and subcooled hydrothermal boiling in groundwater flow channels as a source of harmonic tremor. *Journal of Geophysical Research: Solid Earth*, *93*(B5), 4835-4849.

Maeda, T., Obara, K., Furumura, T., & Saito, T. (2011, October). Interference of long-period seismic wavefield observed by the dense hi-net array in japan. *J. Geophys. Res.*, *116*(B10).

Mardia, K. V., & Jupp, P. E. (1999). *Directional statistics* (K. V. Mardia &

P. E. Jupp, Eds.). Chichester, England: John Wiley & Sons.

Meza-Fajardo, K. C., Papageorgiou, A. S., & Semblat, J.-F. (2015). Identification and extraction of surface waves from Three-Component seismograms based on the normalized inner product. *Bulletin of the Seismological Society of America*, *105*(1), 210–229.

Nakada, S., Nagai, M., Kaneko, T., Suzuki, Y., & Maeno, F. (2013). The outline of the 2011 eruption at shinmoe-dake (kirishima), japan. *Earth, Planets and Space*, *65*(6), 475–488.

Nakamichi, H., Yamanaka, Y., Terakawa, T., Horikawa, S., Okuda, T., & Yamazaki, F. (2013). Continuous long-term array analysis of seismic records observed during the 2011 shinmoedake eruption activity of kirishima volcano, southwest japan. *Earth Planets Space*, *65*(6), 7.

Nakao, S., Morita, Y., Yakiwara, H., Oikawa, J., Ueda, H., Takahashi, H., ... Iguchi, M. (2013). Volume change of the magma reservoir relating to the 2011 kirishima shinmoe-dake eruption—charging, discharging and recharging process inferred from gps measurements. *Earth, Planets and Space*, *65*(6), 505–515.

Nakata, N., Gualtieri, L., & Fichtner, A. (2019). *Seismic ambient noise*. Cambridge University Press.

Reckziegel, F., Bustos, E., Mingari, L., Báez, W., Villarosa, G., Folch, A., ... Osores, S. (2016). Forecasting volcanic ash dispersal and coeval resuspension during the april–may 2015 calbuco eruption. *Journal of Volcanology and Geothermal Research*, *321*, 44-57.

Stockwell, R. G., Mansinha, L., & Lowe, R. P. (1996). Localization of the complex spectrum: the S transform. *IEEE Trans. Signal Process.*, *44*(4), 998–1001.

Swanson, D., Casadevall, T., Dzurisin, D., Holcomb, R., Newhall, C., Malone, S., & Weaver, C. (1985). Forecasts and predictions of eruptive activity at mount st. helens, usa: 1975–1984. *Journal of Geodynamics*, *3*(3), 397-423.

Takagi, R., Nishida, K., Maeda, T., & Obara, K. (2018). Ambient seismic noise wavefield in japan characterized by polarization analysis of hi-net records. *Geophys. J. Int.*, *215*(3), 1682–1699.

Tanimoto, T., Ishimaru, S., & Alvizuri, C. (2006). Seasonality in particle motion of microseisms. *Geophysical Journal International*, *166*(1), 253-266.

Tanimoto, T., & Rivera, L. (2005). Prograde Rayleigh wave particle motion. *Geophysical Journal International*, *162*(2), 399-405.

Yamamoto, M., Kawakatsu, H., Yomogida, K., & Koyama, J. (2001). Long-period (12 sec) volcanic tremor observed at usu 2000 eruption: Seismological detection of a deep magma plumbing system. *Geophysical Research Letters*, *29*. doi: 10.1029/2001GL013996

Yunjun, Z., Amelung, F., & Aoki, Y. (2021). Imaging the hydrothermal system of kirishima volcanic complex with l-band InSAR time series. *Geophys. Res. Lett.*, *48*(11).